

# Multiorbital structure of the two-dimensional electron gas in LaAlO<sub>3</sub>/SrTiO<sub>3</sub> heterostructures: The formation of a $d_{xy}$ ferromagnetic sheet

Jichao C. Li,<sup>1,2</sup> Juan Ignacio Beltrán,<sup>1</sup> and M. Carmen Muñoz<sup>1</sup>

<sup>1</sup>*Instituto de Ciencia de Materiales de Madrid, Consejo Superior de Investigaciones Científicas, ICMM-CSIC, Cantoblanco, 28049 Madrid, Spain*

<sup>2</sup>*School of Physics, Shandong University, Jinan 250100, People's Republic of China*

(Received 16 May 2012; revised manuscript received 17 December 2012; published 7 February 2013)

We demonstrate the formation of a ferromagnetic two-dimensional  $d_{xy}$  electron sheet strictly confined to the TiO<sub>2</sub> interface layer in LaAlO<sub>3</sub>/SrTiO<sub>3</sub> heterostructures. Based on *first-principles* density functional calculations we show that the complex subband structure of the two-dimensional electron gas (2DEG) generated at the LaO/TiO<sub>2</sub> (001) interface is universal, and almost independent of the SrTiO<sub>3</sub> thickness. It is composed of a ladder of  $d_{xy}$  states of light electrons and only one degenerate  $d_{xz,yz}$  heavier subband. All the states are spin polarized although the exchange splitting is only significant for the lowest energy  $d_{xy}$  subband, which leads to magnetic moments ferromagnetically coupled and localized at the interface. The SrTiO<sub>3</sub> ferroelectric-like lattice distortions determine the subband occupation and therefore their orbital character, exchange splitting, and charge density profile. The complex structure of the 2DEG can explain the coexistence in the same sample of superconductivity and magnetism.

DOI: [10.1103/PhysRevB.87.075411](https://doi.org/10.1103/PhysRevB.87.075411)

PACS number(s): 73.20.-r, 73.22.-f, 73.23.-b

## I. INTRODUCTION

The conducting two-dimensional electron gas (2DEG) formed at the LaO/TiO<sub>2</sub> interface between LaAlO<sub>3</sub> and SrTiO<sub>3</sub> insulating oxides,<sup>1</sup> exhibits fundamental collective electronic properties such as superconductivity and magnetism.<sup>2,3</sup> The superconducting phase is similar to that occurring in doped oxygen-deficient bulk SrTiO<sub>3</sub>,<sup>4</sup> while ferromagnetism (FM), has not been observed in either LaAlO<sub>3</sub> or SrTiO<sub>3</sub> doped bulk samples. Moreover, the ferromagnetic phase persists above room temperature (RT) in heterostructures (HS) grown at high oxygen partial pressure,<sup>5</sup> consequently, FM is certainly linked to the presence of interfaces and is unlikely to be associated with oxygen vacancies. The magnetic and superconducting phases were first observed separately in different samples, but recently three different groups have provided direct evidence of the coexistence of the two phenomena in the same sample on a few-micron length scale.<sup>5-8</sup> Nevertheless, whether they coexist in the same region of the samples or there is a phase separation is still a matter of debate. Remarkably, the magnetic moments inferred from torque magnetometry, with the assumption that the signal originates from the SrTiO<sub>3</sub> layer next to the interface, are large: about 0.3–0.4  $\mu_B$  per 2D unit cell (u.c.). Their density is consistent with the interface charge density expected from electrostatic arguments, and their value decreases when the oxygen partial pressure during growth is reduced.<sup>7</sup> Furthermore, it was found that for a 10 u.c. LaAlO<sub>3</sub> layer grown on SrTiO<sub>3</sub>, most of the magnetic dipoles lie in the plane of the interface within a solid angle of  $\pm 30$  degrees and with apparently randomly distributed azimuthal angles.<sup>8</sup> Polarized neutron reflectometry measurements have established an upper limit of 2 G for the averaged magnetization of LaAlO<sub>3</sub>/SrTiO<sub>3</sub> (001) superlattices (SLs).<sup>9</sup> This value is smaller than that obtained by magnetotransport measurements,<sup>7</sup> but it is compatible with the measured magnetic dipoles by direct imaging.<sup>8</sup> In addition, previous band structure calculations show that the strong

correlation effects associated with the Ti  $3d$  orbitals lead to a charge- and spin-ordered insulating ground state, for which both ferromagnetic<sup>10</sup> and antiferromagnetic alignments<sup>11</sup> have been predicted. Geometric confinement has also been invoked to explain the origin of the magnetic conducting state of the (LaAlO<sub>3</sub>)<sub>3</sub>/(SrTiO<sub>3</sub>)<sub>3</sub> superlattice, although for thicker SrTiO<sub>3</sub> layers the magnetic moment decreases and eventually disappears.<sup>12</sup> Moreover, recently oxygen vacancies have been associated with the appearance of magnetism.<sup>13</sup> Nevertheless, dynamical mean-field theory suggests a nonmagnetic ground state.<sup>14</sup> Therefore, the origin of the magnetic phase that emerges at the LaO/TiO<sub>2</sub> interface, but that is exhibited by neither oxide component, is still controversial, and the magnitude of the moments, as well as their orbital character and spatial extent, are undetermined.

In this article, based on first-principles density functional calculations of LaAlO<sub>3</sub>/SrTiO<sub>3</sub> HS, we demonstrate the almost universal subband structure of the 2DEG, and surprisingly the exclusive large spin-polarization of the lowest  $d_{xy}$  subband. The magnetic moments are strictly confined to the TiO<sub>2</sub> interface layer, align ferromagnetically, and lie close to the interface plane. A delicate interplay of quantum confinement, lattice deformation, multiorbital physics, and electron correlation determines the subband structure of the 2DEG with a series of light  $d_{xy}$  and only one  $d_{xz,yz}$  heavy occupied subbands. In particular, the ferroelectric-like structural distortion of the SrTiO<sub>3</sub> drives the occupation of the different subbands, and therefore the SrTiO<sub>3</sub> dielectric constant determines the different mobility and spatial distribution of the different electrons contributing to the 2DEG.

## II. THEORETICAL MODEL

We study ideal defect-free (LaAlO<sub>3</sub>)<sub>*m*</sub>/(SrTiO<sub>3</sub>)<sub>*n*</sub> (001) SLs containing *m* and *n* u.c. of LaAlO<sub>3</sub> and SrTiO<sub>3</sub>, respectively.  $1.5 \leq m \leq 7.5$  and  $7.5 \leq n \leq 17.5$ , *m* and *n* are half-integers,

the SL is symmetric, and it has two identical LaO/TiO<sub>2</sub> interfaces. Density functional calculations are performed using the projector augmented wave method as implemented in the Vienna *Ab initio* Simulation Package (VASP).<sup>15</sup> The exchange-correlation effects were treated within the rotational invariant LSDA +  $U$  approach, which includes a Hubbard  $U$  term accounting for the on-site Coulomb interaction.<sup>16</sup> Ti and Sr semicore  $s$  states are considered as valence states. We performed calculations for different values of the  $U$  and  $J$  exchange parameters for the Ti  $3d$  states, while those for La  $f$  electrons were fixed at 11.0 and 0.68 eV, respectively. Most of the results reported in this article correspond to  $U = 5.0$  and  $J = 0.64$  eV.<sup>17</sup> A kinetic energy cutoff of 500 eV was used and the SL Brillouin zone is sampled with an  $11 \times 11 \times 1$   $k$ -point grid. The lattice constants in the  $x$  and  $y$  directions were fixed to the experimental 3.905 Å SrTiO<sub>3</sub> bulk value, which almost coincides with the calculated equilibrium 3.899 Å parameter, and the  $c$ -axis lattice constant was optimized. All the atomic positions were fully relaxed until atomic forces were smaller than 0.01 eV/Å. The electronic bulk structures of SrTiO<sub>3</sub> and LaAlO<sub>3</sub> are in agreement with previous calculations.

### III. TWO-DIMENSIONAL ELECTRON GAS: MULTIORBITAL STRUCTURE

Figure 1 shows the calculated relaxed-lattice structure for the representative 3.5/8.5 SL. The equilibrium LaAlO<sub>3</sub> lattice constant is 3% smaller than that of SrTiO<sub>3</sub>, therefore it is expected to compress along the  $c$  axis when it is forced to match in-plane to the SrTiO<sub>3</sub>. However, the calculated deviations from the LaAlO<sub>3</sub> out-of-plane lattice constant are small and the structural relaxation occurs primarily in the SrTiO<sub>3</sub> slab, indicating that not only the elastic energy but also interface effects control the SL relaxation. Displacements from the ideal structure do not affect anion and cation equally. There is a ferroelectric-like distortion of the Ti-O octahedra

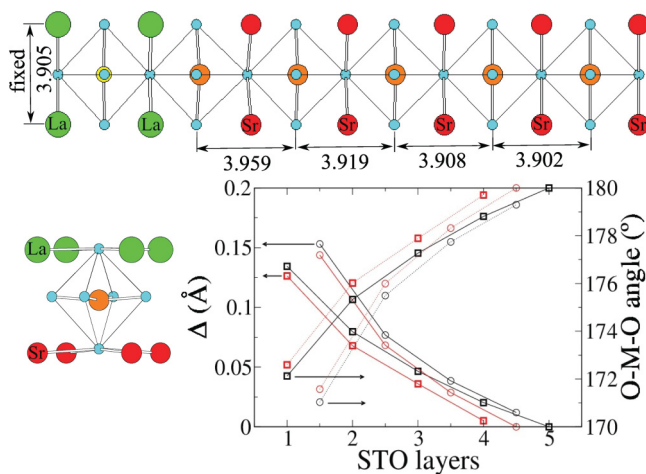


FIG. 1. (Color online) The calculated lattice structure of the 3.5/8.5 SL is represented at the top panel. The distances between the oxygen planes are indicated and only one-half of the u.c. is shown. At the bottom, the polar distortion of the interface TiO<sub>6</sub> octahedron is illustrated. The  $M$ -O displacements and the O- $M$ -O angles [ $M$  = Ti (squares), Sr (circles)], are displayed for the 3.5/8.5 (red symbols) and 7.5/7.5 (black symbols) SLs.

with negatively charged O and positively charged Ti ions moving inward and outward away from the interface layer, respectively. Polar distortions also affect the SrO layers. The relative  $\Delta$  displacements between metal and oxygen atoms are shown in Fig. 1 for two representative SLs. The distortion extends several u.c. from the interface and slightly depends on the SLs periods. The largest  $\Delta$  displacement  $\approx 0.15$  Å occurs at the interface layers. Analogous nonuniform SrTiO<sub>3</sub> lattice polarization has been measured using optical second-harmonic generation<sup>18,19</sup> and also has been predicted theoretically.<sup>20</sup> The off-center displacement of Ti and O atoms is favorable in ferroelectric perovskites and has been also observed in SrTiO<sub>3</sub> surfaces<sup>21</sup> and in Mott-charge transfer LaTiO<sub>3</sub>/SrTiO<sub>3</sub> SLs.<sup>17</sup>

In agreement with previous calculations we find that all the SLs are metallic and a 2DEG emerges at the interface. Since the inhomogeneous Ti-O octahedra distortions give rise to local dipole moments and to a layer-dependent polarization, they may induce changes in the SrTiO<sub>3</sub> band structure and contribute to the formation of the 2DEG. To analyze this effect, we have calculated bulk SrTiO<sub>3</sub> with the frozen structural relaxations corresponding to each layer. In the distorted SrTiO<sub>3</sub> crystals, there is a symmetry-breaking induced ordering of the  $d_{xy}$  orbital, with a  $d_{xy}$ - $d_{xz,yz}$  energy splitting dependent on the distortion. Nevertheless, the SrTiO<sub>3</sub> remains a band insulator for all the range of  $\Delta$  values found in all the SLs investigated. Therefore, in the absence of defects, the charge carriers in the LaAlO<sub>3</sub>/SrTiO<sub>3</sub> HS are only due to the redistribution of charge induced by the SL electrostatic boundary conditions—electronic reconstruction—and they are not caused by the lattice distortions, as occurs in LaTiO<sub>3</sub>/SrTiO<sub>3</sub> SL due to the highly correlated metallic character of tetragonal LaTiO<sub>3</sub>.<sup>22</sup>

Figure 2 illustrates the conduction band (CB) dispersion of the 2DEG for the 3.5/8.5 and 7.5/7.5 SLs. The occupied CB for both SLs is characterized by a set of spin-polarized parabolic subbands corresponding to the  $t_{2g}$  Ti states. The more relevant features are the orbital ordering and the large exchange splitting of the lowest  $d_{xy}$  subband. The intrinsic lower

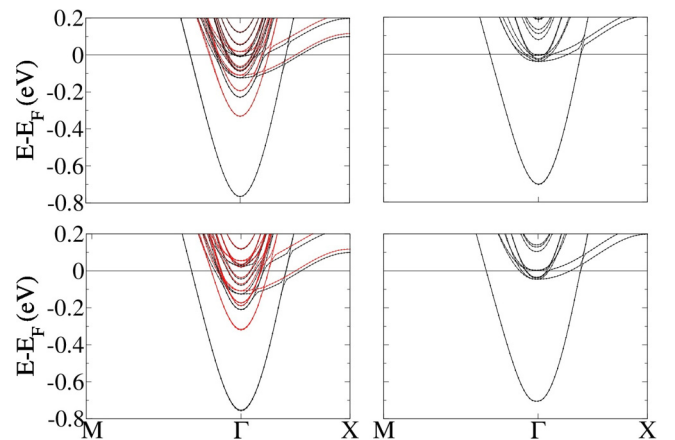


FIG. 2. (Color online) Conduction band near the Fermi energy for the 3.5/8.5 (top) and 7.5/7.5 (bottom) SLs. The left panels correspond to the relaxed structures, while those of the unrelaxed SLs are represented at the right of the figure. Black and red (grey) lines are majority and minority spin states, respectively. The energy zero is located at the Fermi level.

symmetry of the SL crystal field lifts the threefold degeneracy of the  $t_{2g}$  orbitals, which split in the lower nondegenerate  $d_{xy}$  and upper twofold degenerate  $d_{xz,yz}$  subbands. The lower energy of the  $d_{xy}$  subband has been unambiguously established both experimentally<sup>23,24</sup> and theoretically.<sup>20,25–27</sup> The  $d_{xy}$  states are markedly parabolic in the 2D  $k$  space and several subbands are occupied. Contrary, the twofold degenerate  $d_{xz,yz}$  subbands are anisotropic and only one is partially filled in both SLs. The calculated effective masses in the plane parallel to the interface are  $\simeq 0.45$  ( $0.44$ )  $m_e$  for the isotropic  $d_{xy}$  and  $0.71$  ( $0.69$ ) and  $6.20$  ( $5.93$ )  $m_e$  for the anisotropic  $d_{xz,yz}$  bands for the 3.5/8.5 (7.5/7.5) SL. The  $m^*$  of the different subbands compare reasonably with those previously calculated<sup>27</sup> and with the  $1.45$ <sup>28</sup> and  $3.2$   $m_e$  values<sup>29</sup> inferred from transport measurements. Further, they are almost equal to the  $0.5$ – $0.6$   $m_e$  mass of the 2D electron liquid created at the bare SrTiO<sub>3</sub> surface.<sup>30</sup>

#### IV. MAGNETIC ORDER

The more striking characteristic of the CB structure is the large exchange splitting of the lowest  $d_{xy}$  subband:  $0.45$  eV for both 3.5/8.5 and 7.5/7.5 SLs. The splitting decreases as the subband occupation decreases and thus the higher occupied  $d_{xy}$  and the twofold degenerate  $d_{xz,yz}$  subbands slightly contribute to the magnetization. The unbalance of the majority and minority spin states yields a net magnetic moment of  $\approx 0.25$   $\mu_B$  per 2D u.c. for both SLs, in good agreement with the  $0.3$ – $0.4$   $\mu_B$  reported values.<sup>7</sup> Moreover, the magnetic moments are strictly localized in the TiO<sub>2</sub> interface plane and align parallel leading to a ferromagnetic ground state. Analogous features are found for all the SLs investigated, although the splittings and subband occupations slightly depend on the SL period.

The different nature of the  $d_{xy}$  and  $d_{xz,yz}$  Ti  $t_{2g}$  electrons is also manifested in their spatial distribution. Figure 3 shows the charge density profiles along the SL period. Those corresponding to the relaxed SLs are represented at the top panels. The total charge expands across the entire SrTiO<sub>3</sub> slab, although it concentrates preferentially at the interfaces. Nevertheless, the spatial localization depends on the orbital. The  $d_{xy}$  electrons are the major contribution to the density profile and, in agreement with previous calculations, extent only 2 or 3 SrTiO<sub>3</sub> u.c.<sup>20,27</sup> However, the lowest  $d_{xy}$  subband is completely confined to the first TiO<sub>2</sub> layers, whereas higher lying  $d_{xy}$  states increasingly acquires a delocalized nature and spread into the SrTiO<sub>3</sub>. In addition, the maximum probability of the degenerate  $d_{xz,yz}$  band is located at the center of the slab. The calculated density profiles are in good agreement with the reported 1 or 2 nm thickness of the 2DEG,<sup>19,23,24,26</sup> although the magnetic moments—mostly due to the lowest  $d_{xy}$  subband—are confined to the interface.

Thus, our results predict the presence of three different kinds of electrons, which contribute differently to transport and magnetism:

(i) 2D  $d_{xy}$  spin-polarized light carriers confined to the TiO<sub>2</sub> interface plane. They are responsible for the interface magnetism and, due to their confinement, they could be susceptible to localization.<sup>20</sup>

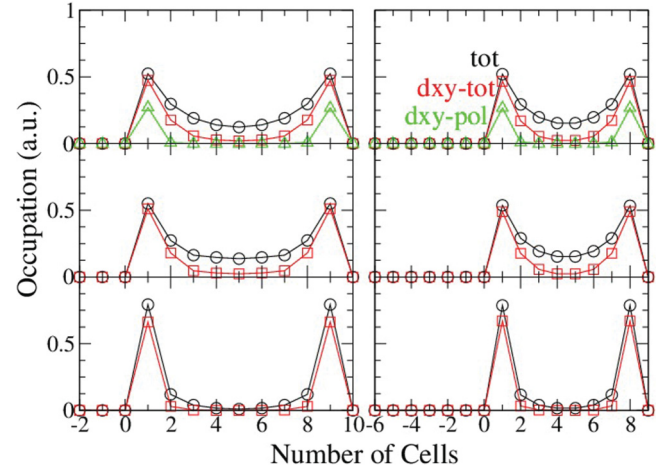


FIG. 3. (Color online) Charge and spin density profiles for the 3.5/8.5 (left panels) and 7.5/7.5 (right panels) SLs. The figure displays the spatial distribution of the total charge (black),  $d_{xy}$  charge (red), and spin (green) density. From top to bottom the calculated densities for the spin-polarized relaxed, non-spin-polarized relaxed, and unrelaxed structures are represented. The two LaO/TiO<sub>2</sub> interfaces are located between 0–1 and 10–9 (9–8) cell numbers for the 3.5/8.5 (7.5/7.5) SL. Therefore, the SrTiO<sub>3</sub> slab ranges between 1 and 9 and between 1 and 8 for the 3.5/8.5 and 7.5/7.5 SLs, respectively.

(ii) Quasi-2D-lying  $d_{xy}$  electrons, also with a light  $m^*$  but spread over several SrTiO<sub>3</sub> layers. Hence, they will present a high mobility and preferentially contribute to the transport.

(iii) And finally quantized  $d_{xz,yz}$  Bloch delocalized carriers with a heavy mass along a planar direction.

Based on experiments an analogous complex subband structure has been recently proposed.<sup>31</sup>

Since negative magnetoresistance (MR) has been measured in LaAlO<sub>3</sub>/SrTiO<sub>3</sub> multilayers, changes in the magnetic orientation seem to have a dramatic effect on the transport properties of the 2DEG.<sup>32</sup> Thus, to examine the magnetocrystalline anisotropy we have performed DFT +  $U$  calculations including the spin-orbit coupling (SOC) for the 3.5/8.5 SL. The major effect of the SOC is local, therefore we considered for simplicity only a Ti per u.c. by replacing the remaining Ti with Al ions, which have no magnetic moment. This procedure avoids any possible coupling between magnetic moments at both interfaces and has been successfully used to calculate the anisotropy of TbMnO<sub>3</sub>.<sup>33</sup> The dependence of the total energy on the Ti spin direction obtained from the DFT +  $U$  + SOC calculations is shown in Fig. 4. The energy minimum occurs at  $135^\circ$  from the SL growth direction; that is,  $45^\circ$  deviated from the interface plane. Experimentally it was found that, in a 10 u.c. LaAlO<sub>3</sub> layer grown on SrTiO<sub>3</sub>, most of the dipoles lies in the plane of the interface within a solid angle of  $\pm 30$  degrees and with apparently randomly distributed azimuthal angles.<sup>8</sup> The discrepancy found in our calculation may be due to the large contribution in the experiments of the shape anisotropy, which tends to align the magnetization on the plane. Nevertheless both results indicate that the magnetocrystalline contribution is not perpendicular to the interface as often occurs in ultrathin layers of magnetic metals.<sup>34</sup>

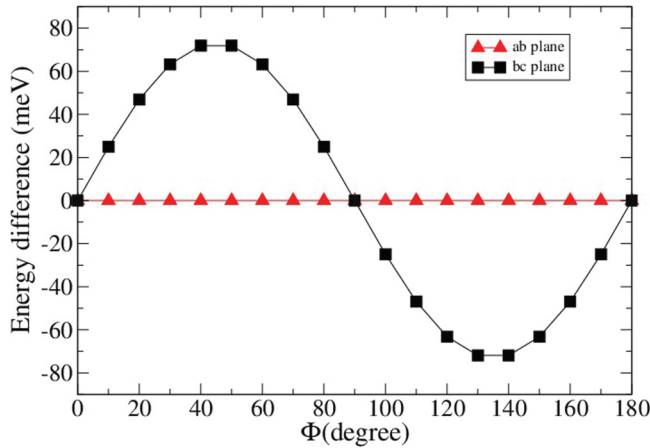


FIG. 4. (Color online) Anisotropy energy as a function of the spin direction with respect to the normal to the interface for a 3.5/8.5 SL (an angle of  $90^\circ$  means the magnetization lies in the plane of the interface).

In order to investigate the origin of the predicted magnetization we calculate the relaxed SLs without spin-polarization. The energy of the non-spin-polarized SLs is higher by  $\simeq 25$  meV per formula unit for both SLs.

The corresponding charge density profiles are represented in the middle panels of Fig. 3. They are similar to those of the spin-polarized calculations, indicating that the spin polarization does not alter significantly the occupation of the different  $t_{2g}$  subbands, thus its effect is to reduce the total energy of the SLs. Electrons occupying the spin-polarized bands reduce their energy due to the balance of the kinetic and Coulomb contributions.

Figure 3 also displays the density profiles of the unrelaxed SLs. They show the almost complete confinement of the electrons to the  $\text{TiO}_2$  interface plane, with only a very small amount spread into the next  $\text{TiO}_2$  layers. Furthermore, almost all the electrons have a  $d_{xy}$  orbital character, as is also clearly appreciated in the left panels of Fig. 2, where the corresponding CBs are represented. Most of the charge is accommodated in the lowest  $d_{xy}$  state, with a very small proportion occupying highest subbands. Surprisingly, all the subbands are non-spin-polarized, despite spin polarization being allowed in the calculations. The system remains in a zero-spin state and, due to the large interface crystal field  $d_{xy}$ ,  $d_{xz,yz}$  induced splitting, there is a preferential filling of the lowest  $d_{xy}$  subband. The calculated energy gain due to the lattice relaxation is large  $\simeq 0.46$  eV per formula unit, one order of magnitude greater than the  $\simeq 25$  meV due to the spontaneous spin polarization. The large charge density concentrated at the interface plane in the unrelaxed SLs must be unstable and

the nonuniform lattice polarization emerges as a response of the system. The ferroelectric-like distortion induced in the relaxation promotes the occupation of higher bands and thus the delocalization of the charge over the  $\text{SrTiO}_3$  slab.

In addition, we have also performed calculations with different values of  $U$ ; only for  $U \geq 2$  eV a spin polarization is spontaneously induced and the ferromagnetic solution is more stable. Both the magnetic moment and the magnetic energy increase with the value of  $U$ . Therefore, electron correlation is essential to stabilize the magnetic state, although in the absence of lattice distortions it is not enough to promote the magnetic state.

## V. CONCLUSION

To summarize, on the basis of DFT calculations we found that the  $\text{SrTiO}_3$  dielectric properties determine the charge density distribution of the 2DEG, since ion displacements from their centrosymmetric positions in the  $\text{TiO}_6$  octahedra are essential to promote the occupation of delocalized bands. Therefore, the subband structure of the 2DEG is almost universal and is composed of a ladder of  $d_{xy}$  states with a light effective mass and only one degenerate  $d_{xz,yz}$  heavier subband. Electron correlation induces the spontaneous spin polarization of  $\text{Ti } t_{2g}$  subbands, although only the lowest  $d_{xy}$  subband contributes substantially to the magnetic moments, which are confined to the interface.

The interplay of lattice deformation, multiorbital physics, quantum confinement, and electron correlation determines the SL ground state. All are crucial factors promoting the magnetic state. The cooperative action of lattice, orbital and spin degrees of freedom together with disorder—not considered in our calculations—can lead to nanoscale charge inhomogeneities. This together with the small free energy differences between different states—e.g.,  $\simeq 25$  meV between the magnetic and non-magnetic solution for  $U = 5$  eV—can explain the diverse experimental observations and even more the coexistence of spatial inhomogeneities in the sample. Therefore, the different kinds of carriers contributing to the 2DEG can explain the coexistence of superconductivity and magnetism in the same sample.

## ACKNOWLEDGMENTS

This work has been supported by the Spanish Ministry of Science and Technology (MICI) under Grant No. MAT2009-14578-C03-03, and by the CSIC Intramural project 201060E041. J.L. acknowledges financial support from the Spanish Estancias de Jóvenes Doctores Extranjeros program. Computations were performed at the Supercomputing Centre of Galicia (CESGA).

<sup>1</sup>A. Ohtomo and H. Y. Hwang, *Nature (London)* **427**, 423 (2004).

<sup>2</sup>N. Reyren, S. Thiel, A. D. Caviglia, L. F. Kourkoutis, G. Hammerl, C. Richter, C. W. Schneider, T. Kopp, A.-S. Retschi, D. Jaccard *et al.*, *Science* **317**, 1196 (2007).

<sup>3</sup>A. Brinkman, M. Huijben, M. van Zalk, J. Huijben, U. Zeitler, J. C. Maan, W. G. van der Wiel, G. Rijnders, D. H. A. Blank, and H. Hilgenkamp, *Nat. Mater.* **6**, 493 (2007).

<sup>4</sup>J. F. Schoolley, W. R. Hosler, and M. L. Cohen, *Phys. Rev. Lett.* **12**, 474 (1964).

- <sup>5</sup>Ariando, X. Wang, G. Baskaran, Z. Q. Liu, J. Huijben, J. B. Yi, A. Annadi, A. R. Barman, A. Rusydi, S. Dhar *et al.*, *Nat. Commun.* **2**, 188 (2011).
- <sup>6</sup>D. A. Dikin, M. Mehta, C. W. Bark, C. M. Folkman, C. B. Eom, and V. Chandrasekhar, *Phys. Rev. Lett.* **107**, 056802 (2011).
- <sup>7</sup>L. Li, C. Richter, J. Mannhart, and R. C. Ashoori, *Nat. Phys.* **7**, 762 (2011).
- <sup>8</sup>J. A. Bert, B. Kalisky, C. Bell, M. Kim, Y. Hikita, H. Y. Hwang, and K. A. Moler, *Nat. Phys.* **7**, 767 (2011).
- <sup>9</sup>M. R. Fitzsimmons, N. W. Hengartner, S. Singh, M. Zhernenkov, F. Y. Bruno, J. Santamaria, A. Brinkman, M. Huijben, H. J. A. Molegraaf, J. de la Venta *et al.*, *Phys. Rev. Lett.* **107**, 217201 (2011).
- <sup>10</sup>R. Pentcheva and W. E. Pickett, *Phys. Rev. B* **74**, 035112 (2006).
- <sup>11</sup>Z. Zhong and P. J. Kelly, *Europhys. Lett.* **84**, 27001 (2008).
- <sup>12</sup>K. Janicka, J. P. Velev, and E. Y. Tsymbal, *J. Appl. Phys.* **103**, 07B508 (2008).
- <sup>13</sup>N. Pavlenko, T. Kopp, E. Y. Tsymbal, G. A. Sawatzky, and J. Mannhart, *Phys. Rev. B* **85**, 020407 (2012).
- <sup>14</sup>C.-K. Chan, P. Werner, and A. J. Millis, *Phys. Rev. B* **80**, 235114 (2009).
- <sup>15</sup>G. Kresse and J. Hafner, *Phys. Rev. B* **47**, 558 (1993). G. Kresse and J. Furthmüller, *ibid.* **54**, 11169 (1996). G. Kresse and D. Joubert, *ibid.* **59**, 1758 (1999).
- <sup>16</sup>V. I. Anisimov, F. Aryasetiawan, and A. I. Lichtenstein, *J. Phys.: Condens. Matter* **9**, 767 (1997).
- <sup>17</sup>S. Okamoto, A. J. Millis, and N. A. Spaldin, *Phys. Rev. Lett.* **97**, 056802 (2006).
- <sup>18</sup>N. Ogawa, K. Miyano, M. Hosoda, T. Higuchi, C. Bell, Y. Hikita, and H. Y. Hwang, *Phys. Rev. B* **80**, 081106 (2009).
- <sup>19</sup>A. Rubano, M. Fiebig, D. Paparo, A. Marino, D. Maccariello, U. Scotti di Uccio, F. Miletto Granozio, L. Marrucci, C. Richter, S. Paetel *et al.*, *Phys. Rev. B* **83**, 155405 (2011).
- <sup>20</sup>Z. S. Popović, S. Satpathy, and R. M. Martin, *Phys. Rev. Lett.* **101**, 256801 (2008).
- <sup>21</sup>E. Heifets, R. I. Eglitis, E. A. Kotomin, J. Maier, and G. Borstel, *Phys. Rev. B* **64**, 235417 (2001).
- <sup>22</sup>H. Ishida and A. Liebsch, *Phys. Rev. B* **77**, 115350 (2008).
- <sup>23</sup>M. Salluzzo, J. C. Cezar, N. B. Brookes, V. Bisogni, G. M. De Luca, C. Richter, S. Thiel, J. Mannhart, M. Huijben, A. Brinkman *et al.*, *Phys. Rev. Lett.* **102**, 166804 (2009).
- <sup>24</sup>M. Sing, G. Berner, K. Goß, A. Müller, A. Ruff, A. Wetscherek, S. Thiel, J. Mannhart, S. A. Pauli, C. W. Schneider *et al.*, *Phys. Rev. Lett.* **102**, 176805 (2009).
- <sup>25</sup>W.-J. Son, E. Cho, B. Lee, J. Lee, and S. Han, *Phys. Rev. B* **79**, 245411 (2009).
- <sup>26</sup>M. Stengel, *Phys. Rev. Lett.* **106**, 136803 (2011).
- <sup>27</sup>P. Delugas, A. Filippetti, V. Fiorentini, D. I. Bilc, D. Fontaine, and P. Ghosez, *Phys. Rev. Lett.* **106**, 166807 (2011).
- <sup>28</sup>A. D. Caviglia, S. Gariglio, C. Cancellieri, B. Sacépé, A. Fête, N. Reyren, M. Gabay, A. F. Morpurgo, and J.-M. Triscone, *Phys. Rev. Lett.* **105**, 236802 (2010).
- <sup>29</sup>A. Dubroka, M. Rössle, K. W. Kim, V. K. Malik, L. Schultz, S. Thiel, C. W. Schneider, J. Mannhart, G. Herranz, O. Copie *et al.*, *Phys. Rev. Lett.* **104**, 156807 (2010).
- <sup>30</sup>W. Meevasana, R. H. He, S.-K. Mo, M. Hashimoto, A. Tamai, P. Songsiririthgul, F. Baumberger, and Z.-X. Shen, *Nat. Mater.* **10**, 114 (2011).
- <sup>31</sup>H. Y. Hwang, in *Frontiers in Electronic Materials: Correlation Effects and Memristive Phenomena* (Aachen, Germany, 2012) (unpublished).
- <sup>32</sup>M. Ben Shalom, C. W. Tai, Y. Lereah, M. Sachs, E. Levy, D. Rakhmilevitch, A. Palevski, and Y. Dagan, *Phys. Rev. B* **80**, 140403 (2009).
- <sup>33</sup>H. J. Xiang, S.-H. Wei, M.-H. Whangbo, and J. L. F. Da Silva, *Phys. Rev. Lett.* **101**, 037209 (2008).
- <sup>34</sup>F. El Gabaly, S. Gallego, C. Muñoz, L. Szunyogh, P. Weinberger, C. Klein, A. K. Schmid, K. F. McCarty, and J. de la Figuera, *Phys. Rev. Lett.* **96**, 147202 (2006).